Water Research X 19 (2023) 100175

Contents lists available at ScienceDirect

Water Research X

journal homepage: www.sciencedirect.com/journal/water-research-x

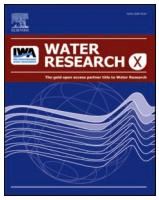

Molecular framework for designing Fluoroclay with enhanced affinity for per- and polyfluoroalkyl substances

Bei Yan [a,*], Jinxia Liu [a,*]

[a] Department of Civil Engineering, McGill University, 817 Sherbrooke Street West, Montreal, Quebec H3A 0C3, Canada

ARTICLE INFO

Keywords:
Density functional theory
Molecular dynamics
Per- and Polyfluoroalkyl Substances
Rational designing
Self-assembly

ABSTRACT

Motivated by the need for enhancing sorbent affinity for per- and polyfluoroalkyl substances (PFAS), we demonstrate the possibility of rationally designing clay-based material (FluoroClay) with a pre-selected intercalant and predicting sorbent performance using all-atom molecular dynamics simulation coupled with density functional theory-based computation. Perfluorohexyldodecane quaternary ammonium (F6H12A) as the selected intercalant revealed significant enhancement in adsorption affinity for hard-to-remove compounds, including perfluorobutane sulfonate (PFBS) and polyfluoroalkylethers (GenX and ADONA). The adsorption is thermodynamically entropy-driven and dominated by the hydrophobic effect. The incorporation of fluorine atoms into clay intercalants gave rise to a hydrophobic and fluorophilic "cavity" structure for targeted PFAS. The self-assembly of intercalant-PFAS under the negative electric field of clay sheets created a unique configuration that significantly enlarged the contact surface area between PFAS and F6H12A and was quantitatively driven by their intermolecular interactions, e.g., CF chain-CH chain, CF chain-CF chain, and charge-CH chain interactions. Collectively, our work demonstrated a new approach to select fluorinated functionality for designing a new adsorbent and estimating its performance via molecular simulation. It also provided an in-depth understanding of the underlying fundamental physics and chemistry in the adsorption of PFAS, suggesting a new strategy for PFAS removal, particularly for short-chain PFAS and new chemical alternatives.

Introduction

Water contamination by per- and polyfluoroalkyl substances (PFAS) impacts many countries and leads to regulatory actions to reduce human exposure to these toxic chemicals (Backe et al., 2013; Houtz et al., 2013; Moody et al., 2003; Munoz et al., 2018; Munoz et al., 2023). PFAS are used to make water and oil repellent coatings, specialty polymers, pesticides, and aqueous film-forming foams (AFFF) for controlling class B fires (Buck et al., 2011; Kissa, 2001). However, the strong C-F single bond (av. ~485 kJ/mol) and F being a hard atom (Krafft and Riess, 2015) that make PFAS versatile in applications also lead to persistent pollutants. Drinking water guidelines as low as 0.004 ng/L for perfluorooctane carboxylate (PFOA) and 0.02 ng/L perfluorooctane sulfonate (PFOS) are developed by U.S. EPA (2022). The long-chain PFAS remain widely detected despite phase-out, while replacements with short perfluoroalkyl chains (e.g., perfluorobutane sulfonate, PFBS) or alternative chemistry (e.g., polyfluoroalkylether) pose emerging concerns and are highlighted in the newly released "PFAS Strategic Roadmap: EPA's Commitments to Action 2021-2024" (U.S. EPA, 2021). Stringent guidelines result in costly water treatment processes because existing adsorbents used for removing PFAS from water are often not effective.

The most commonly used activated carbon relies on large specific surface areas among a porous structure and the hydrophobic effect to remove organics of low solubility from water. However, activated carbon shows limited efficacy for removing short-chain PFAS ($n < 6$) because of the high solubility imparted by charged functional groups (e.g., carboxylate, sulfonate). Alternatively, adsorbents that enable ion exchange processes (or ionic interactions) are utilized to remove anionic PFAS. Such adsorbents are either functionalized with amine groups (e.g., diethylaminoethyl, quaternary amine) or are inherently aminated (e.g., polyacrylonitrile). However, the competitive adsorption from co-existing organic (e.g., humic and fulvic acids) and inorganic (e.g., sulfate, chloride) anions, at concentrations of magnitude higher than PFAS, can significantly reduce the efficacy of the ion exchange process in removing PFAS (Ateia et al., 2019; Boyer et al., 2021; Kumarasamy et al., 2020). Alternatively, Xiao et al. (2017) and Yang et at. (2020) crosslinked fluorinated substituents (e.g., decafluorobiphenyl and tris

* Corresponding authors.
E-mail addresses: bei.yan@mail.mcgill.ca (B. Yan), jinxia.liu@mcgill.ca (J. Liu).

https://doi.org/10.1016/j.wroa.2023.100175
Received 9 January 2023; Received in revised form 7 March 2023; Accepted 8 March 2023
Available online 11 March 2023

(2-aminoethyl)amine with pentafluorobenzaldehyde) with structures of β-cyclodextrin-containing polymers and reported greater affinity for PFOA than activated carbon or non-fluorinated. Du et al. (2016) modified montmorillonite with a cationic fluorosurfactant and attributed enhanced adsorption of PFOS/PFOA to fluorophilic interactions between C-F chains of the intercalants and target contaminants. These studies have inspired us to explore adding fluorinated substituents into adsorbents and using the C-F chain and related molecular interactions for PFAS water treatment.

However, no theoretical framework or empirical methods exist for selecting fluorinated functionality for creating new adsorbents for water treatment. As laboratory evaluation of adsorbent performance is tedious and costly, we chose molecular dynamics simulation and Density Functional Theory (DFT) computation to address this challenge. All-atom molecular dynamics (MD), a simulation method based on classical mechanics of multiparticle systems, can provide the ultimate details of particles (e.g., atoms, groups, and molecules), offering a "seeing is believing" way of studying their physical movements (Adcock and McCammon, 2006). Furthermore, a detailed and accurate picture of how PFAS molecules interact can also be attained by the DFT-based quantum computations, which determine atomic forces and system energy from first principles by approximating the Schrödinger equation (Hermann et al., 2017). Previously, these tools have been complementarily used to support laboratory investigations by elucidating adsorption mechanisms and reaction pathways, including for the uptake of PFAS by various adsorbents (Yan et al., 2020; Yan et al., 2021) and defluorination of PFAS with hydrated electrons (Biswas et al., 2022; Yamijala et al., 2020). Herein, we propose that this powerful coupled simulation tool is also suitable for the rational design of new adsorbents with fluorinated functionalities (FluoroClay) before material synthesis and laboratory testing are to be conducted. In this proof-of-concept study, we choose smectite clay as the substrate for functionalization. The layered material has been used to create organic-inorganic nanocomposites through intercalating organic species (e.g., neutral molecules, organic cations, or anions) in the exchange sites of interlayer space. The presence of clay can improve the mechanical, thermal, barrier and fire retardancy properties of these organic species (Ruiz-Hitzky and Van Meerbeek, 2006). Smectite is suitable for water treatment also due to practical reasons, e.g., low cost, durability, large interlayer space, and fouling resistance (Cadars et al., 2012; Zeng et al., 2003). Besides developing the theoretical framework, the study reveals in-depth molecular mechanisms involving a range of fluorinated structures.

Designing intercalant for PFAS through advanced computations

The starting point was to compare the relative magnitude of hydrophobic and fluorophilic interactions that major PFAS can engage. Previous experiments demonstrated that the adsorbent capacity increases with increased perfluoroalkyl (CF) chain length (Park et al., 2020). From this premise, DFT-based computations were carried out to determine the free energy of solvation for anionic PFAS in water, n-octanol, and 2,2,2-trifluoroethanol (at pH 7). The widely used B3LYP method with the SMD model was chosen (Liu et al., 2018), and the dispersion interactions were also included via the D3 version of Grimmer's dispersion (Grimme et al., 2010). Three most common basis sets, e.g., 6311++Gdp, 6311++G2d2p, and 6311+G3df2p, were tested, and the values determined at 6311+G3df2p, which shows the smallest average bond length differences (theory - experiment) of 398 molecules (U.S. NIST, 2022), were set as the benchmarking data (Fig. S1 and Table S1-S3). Hidalgo and Mora-Diez (2016) compared the partitioning coefficients of perfluoroalkyl carboxylic acids (PFCA) predicted by DFT theory with experimental data determined by Jing et al. (2009), and found that the general trend could be well reproduced using DFT-based computation, though the Log*P* values for the carboxylates were underestimated with average errors of -2.74. Therefore, we focused on the trend (slope, i.e., increase in log unit per CF_2). The 11 representative structures included six perfluoroalkyl sulfonates (PFSAs, e.g., PFBS, PFPeS, PFHxS, PFHpS, PFOS, and PFNS), one carboxylate (PFOA), one fluorotelomer sulfonate (6:2 FtSA), one sulfonamide (FHxSA), and two polyether carboxylates, GenX (hexafluoropropylene oxide dimer acid) and ADONA (4,8-dioxa-3H-perfluorononanoate). The slope of basis set 6311++Gdp was determined to be 0.50, which is close to 0.51 of 6311+G3df2p, and the residual sum of squares of 6311++Gdp was small (0.12) (Fig. S2), thus 6311++Gdp was chosen as the basis set for DFT-based computations in this study. The corresponding hydrophobicity and fluorophilicity were predicted by the distribution coefficient LogD_{OW} (octanol-water) and LogD_{FW} (2,2,2-trifluoroethanol-water) (Fig. 1b). Take PFSAs as examples, LogD_{OW} and Log D_{FW} increased with increased CF chain length, showing enhanced hydrophobicity and fluorophilicity, except for PFNS having a slightly lower LogD_{FW} than PFOS. For a specific PFAS, the LogD_{FW} value is ~1.6 log units larger than LogD_{OW}, suggesting that PFAS favor fluorous phase/domain more than hydrocarbon phase/domain. Encouraged by this calculation, we tested a fluorinated analog to a common hydrocarbon quaternary ammonium intercalant (C18, H$(CH_2)_{18}N^+(CH_3)_3$) by partially replacing CH segment with CF; F6H12A ($F(CF_2)_6(CH_2)_{12}N^+(CH_3)_3$ perfluorohexyldodecane quaternary ammonium) was selected as the hypothetical fluorinated intercalant after we evaluated the influence of n ($4 \leq n \leq 12$) in $F_nH_{12}A$ (discussed in Supporting Information, Fig. S3-S12 and Table S4)

To assess the effect of such a modification, we conducted microsecond-long fully atomistic MD simulations for 12 intercalants and 1 PFAS in the interlayer of 6 × 4 clay supercells immersed in explicit SPC/E water (Berendsen et al., 1987). The density distributions of the headgroup group (i.e., quaternary ammonium), CH chain, and CF chain of the intercalants (C18 and FnH12A) in the direction normal to the clay surface were calculated to establish the interlayer structure in C18/FnH12A-clay. The initially randomly oriented C18 or F6H12A intercalants spontaneously self-assembled into cylinder aggregates or hemimicelles. Under the negative electric field (the smectite layer is naturally negatively charged due to the iso-substitution of Al by Mg), the positively charged ammonium groups headed to silicate layers, as seen in the two sharp peaks in the density profiles in Fig. 2a, 2c, 2e, and 2g, while the CH or CF-CH chains twisted in the center of interlayer and formed hydrophobic domains revealed by the dramatic drops in water density. The root means square deviation (RMSD) levels of intercalants and PFBS were about 0.35 and 0.1 nm (Fig. S13), indicating the structures were very stable. Notably, all PFAS (the interlayer structure of PFPeS, PFHpS, PFNS, PFOA, 6:2 FtSA, FHxSA, GenX, ADONA were given in Fig. S14) participated in the aggregate and were wrapped in the CF-CH domain of F6H12A (Fig. 2d, 2f, and 2h), which implied strong intermolecular affinity. Conversely, PFBS interacted with the surface of C18 aggregate and was largely in contact with the water phase, as illustrated in Fig. 2b. The simulation results demonstrate that the adsorption of PFAS in the interlayer of (modified) smectite clay experienced self-assembly of fluorinated intercalant-PFAS under the negative electric field of clay sheets.

Driving force, interaction strength, and orbital origin of PFAS-intercalant self-assembly

A DFT-based thermochemistry calculation was performed to investigate the driving force of such a spontaneous self-assembly behavior; the focus is on the intercalant-PFAS with C18-PFBS and F6H12A—PFBS as examples. The water cage (i.e., hydration) was taken into account (Phillips, 1955). Due to the limit of computational resources, 24 clay unit cells that strongly interacted with the quaternary ammonium headgroup rather than the hydrophobic domain (Zeng et al., 2003) were not included, and the number of 12 F6H12A intercalants was reduced to 3. Three configurations of 3C18—1PFBS (Fig. S15) and 3F6H12A—1PFBS (Fig. 2i) were obtained from the last 10 ns of the above 1 μs MD simulation. The RMSD levels of intercalant and PFBS were off to 0.35 and 0.1 nm, respectively, indicating the structures were

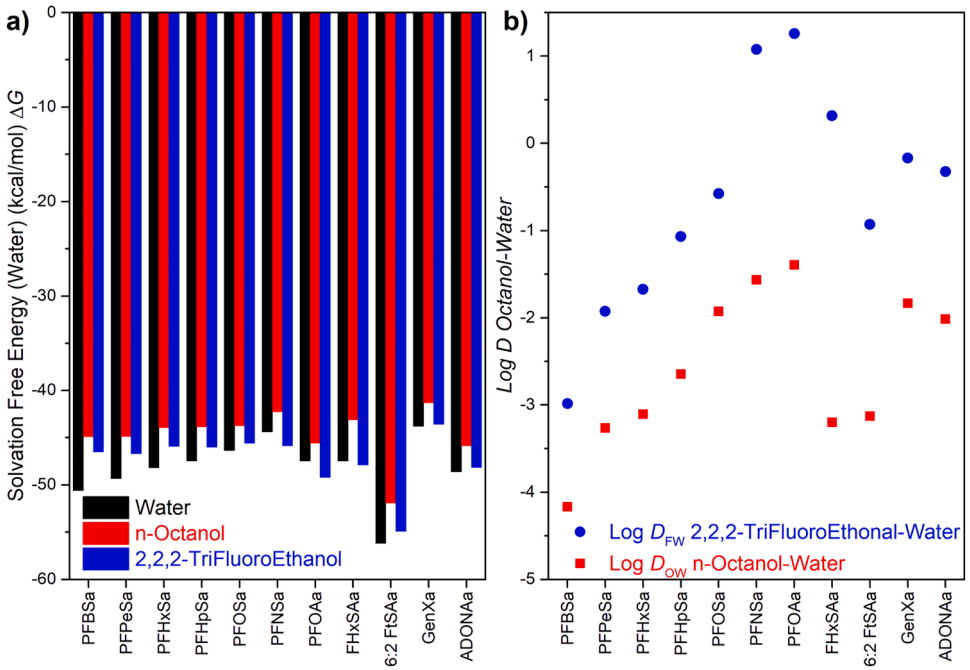

Fig. 1. a) Solvation free energy of PFAS in water, n-octanol, and 2,2,2-trifluoroethanol; b) calculated octanol-water and 2,2,2-trifluoroethanol-water distribution coefficients of PFAS at the B3LYP/6311++Gdp level of theory with GD3 dispersion correction using SMD as the solvation model. All PFAS were geo-optimized with the frequency check.

very stable (Fig. S13). The thermochemistry analysis was divided into two steps to compare with the reference data of micellization (Phillips, 1955): (1st step) self-assembly of the three intercalants, and (2nd step) PFBS contacting or entering the self-assembly structure. The change in Gibbs free energy (ΔG_1) of step 1 were determined: 3C18—1PFBS, -34.41 kcal/mol; and 3F6H12A—1PFBS, -54.25 ± 4.60 kcal/mol (details in Table S5-S8). Therefore, the Gibbs free energy gained per C18/F16H12A entering the self-assembly structure formed by the intercalants were determined to be -11.47 and -18.08 ± 1.53 kcal/mol (i.e., $\Delta G_1/3$), which were highly consistent with the benchmarking values (for a C18 13.43 kcal/mol; and for F6H12A 16.26-17.28 kcal/mol) predicted by Phillips (1955). In the 2nd step, the ΔG_2 of 3F6H12A for one PFBS (-108.07 ± 7.90 kcal/mol) was 4.4 times larger than that of 3C18 (-24.57 kcal/mol), indicating the structure formed by 3F6H12A was more favorable for adsorbing PFBS than that of 3C18. The ΔG and ΔH with hydration, in sum, were 3C18-1PFBS, -58.98 and -22.55 kcal/mol; and 3F6H12A—1PFBS, -162.32 and -40.30 kcal/mol. In contrast, without the water cages, the corresponding ΔG values were 15.17 and 37.02 ± 11.98 kcal/mol, respectively. The hydrophobic effect arising from the release of low entropy hydration water into bulk solution during the self-assembly of 3F6H12A—1PFBS could be further quantified: ΔG = -199.34 ± 6.38 kcal/mol, ΔH = -24.5 ± 14.83 kcal/mol, and $T{\cdot}\Delta S$ = 174.84 ± 8.79 kcal/mol. The results revealed that the self-assembly of intercalant-PFAS was thermodynamically entropy-driven and dominated by the hydrophobic effect, in agreement with Phillips (1955) and Maestre et al. (2014).

Though the self-assemblies of C18—PFAS and F6H12A—PFAS are both spontaneous and governed by hydrophobic effect, the distinct aggregate structures of F6H12A—PFAS originated from the enhanced intermolecular interactions between F6H12A and PFAS largely intensified such as an effect. To probe the interactions, we mapped the electrostatic potential onto the electron isodensity surface of C18—PFBS, F6H12A—PFBS, F6H12A—PFHxS, F6H12A—PFOS (extracted from Fig. 2b, 2d, 2f, and 2g), as illustrated in Fig. 3a, 3b, 3c, and 3d. The orientations of PFBS, PFHxS, and PFOS within the CF-CH domain of F6H12A correlate with the alignment between high electron density regions (blue area) and poor electron density (red area). This pattern seemed to be particularly crucial in F6H12A—PFAS aggregates, where the electron-rich region (anionic sulfonic group; CF chain of PFAS) and the electron-poor region (CH chain of 12 F6H12A) generated a total permanent dipole across the CF-CH domain (i.e., 12F6H12A—1PFBS) of 2373 D. PFBS in 12 F6H12A had a dipole moment of 210 D, and its vector was antiparallel to the dipole of the 12F6H12A (2581 D) upon the formation of 12F6H12A—1PFBS aggregate. Analogous results could be observed in 12F6H12A—1PFHxS and 12F6H12A—1PFOS (Table S9). 12C18 in the aggregate with PFBS revealed a much larger permanent dipole (4433 D) compared to 12F6H12A (in aggregate with PFBS), and the dipole vector of PFBS in the aggregate 12C18-1PFBS was not particularly aligned with the dipole of 12C18. The dipole reproducibility was confirmed for 12C18—1PFBS and 12F6H12A—1PFBS systems with longer MD simulation times, e.g., 2 μs, 3 μs, and 5 μs (Table S9).

To quantify the association strength between intercalant and PFAS, we determined the multiple interaction energies (ΔE) between the moieties of 12C18 (or 12F6H12A) with those of PFAS: ((PFAS) CF chain-CF chain (of intercalant), CF chain-CH chain, and CF chain-charge (of intercalant, $-CH_2-N^+(CH_3)_3$); PFAS charge-intercalant: (head group of PFAS, $-COO^-$, $-SO_3^-$, or $-SO_2NH^-$) charge-CF chain (of intercalant), charge-CH chain, and lastly charge-charge. As shown in Fig. 3e, F6H12A had a much larger ΔE (~ 1.8 times) with PFBS than C18 due to the remarkable "cavity" structure formed by the CH-CF domain. The trend among the PFAS homologue shows that a longer CF chain corresponds to a higher ΔE because of a larger contacting surface area and more CF_2 dipoles. Namely, PFNS (48.1 kcal/mol) demonstrated the strongest interaction with F6H12A, followed by PFOS (44.3 kcal/mol), 6:2 FtSA (42.2 kcal/mol), PFOA (37.9 kcal/mol), FHxSA (37.1 kcal/mol), and PFHxS (36.1 kcal/mol). The trend is consistent with the reported trend of PFAS adsorption (Du et al., 2016; Yan et al., 2020). Furthermore, F6H12A strongly interacted with GenX (38.3 kcal/mol) and ADONA (35.7 kcal/mol), implying its application potential for the emerging PFAS. Interestingly, dipole-dipole interactions involving CF chain (i.e., CF chain-CH chain and CF chain-CF chain) contributed to a large proportion of the total ΔE, particularly the CF chain-CH chain that may be caused by the impact of introduced CF chain on the CH chain of F6H12A (Krafft and Riess, 2009, 2015). Instead, the contribution of the positively

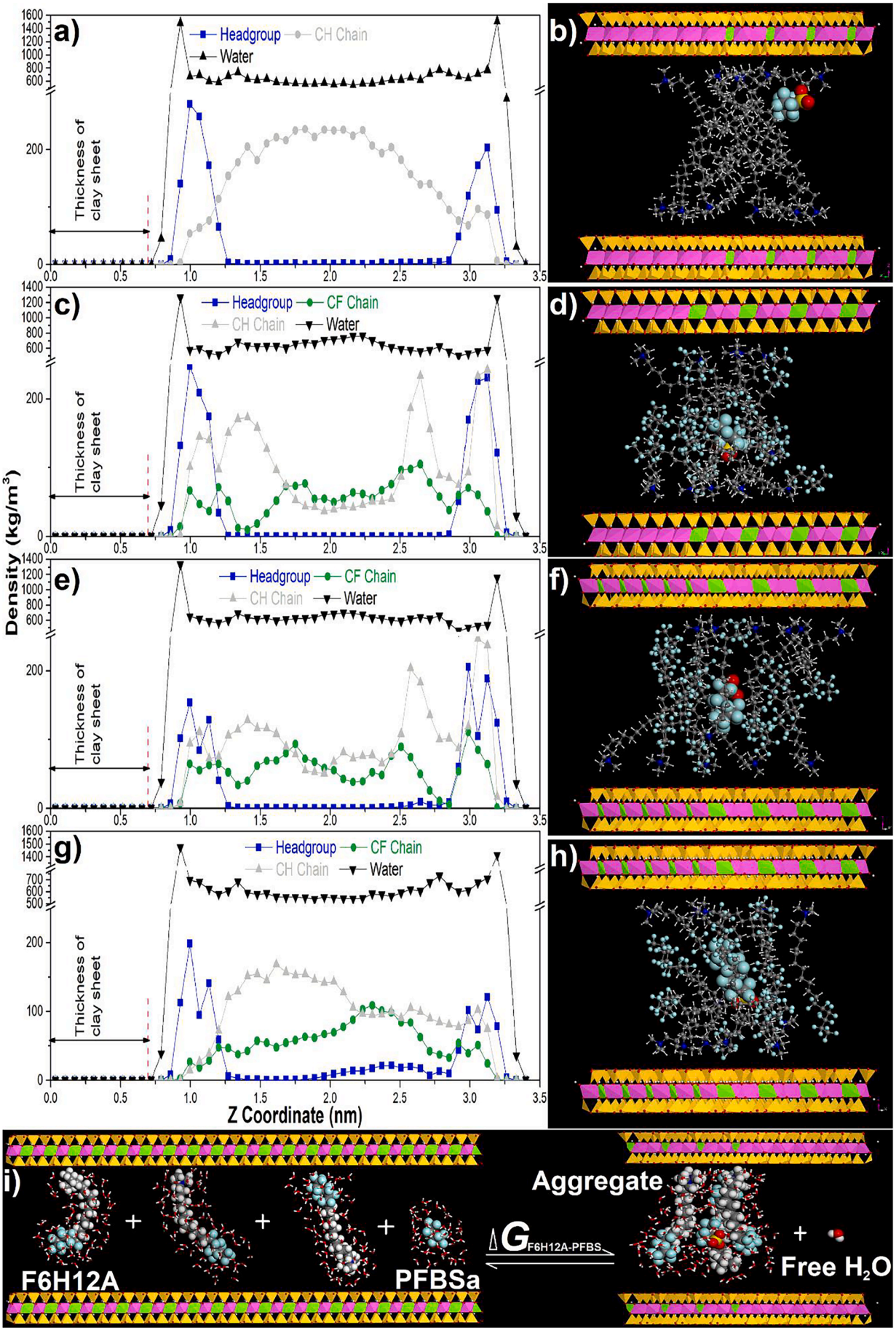

(caption on next page)

Fig. 2. Density distributions of the headgroup, CF chain, CH chain, and water of 12C18-1PFBS (a), 12F6H12A—1PFBS (c), 12F6H12A—1PFHxS (e), 12F6H12A—1PFOS (g) in the last 10 ns, and the corresponding snapshots b), d), f) and h) at 1 μs MD simulation, water omitted for clarity; i) reaction scheme of 3F6H12A—1PFBS aggregate formed by 3 F6H12A and 1 PFBS surrounded by water molecules, $1F6H12A\bullet 39H_2O$ $+1F6H12A\bullet 39H_2O$ $+1F6H12A\bullet 46H_2O$ $+1PFBS\bullet 13H_2O \Leftrightarrow^{\Delta G}$ aggregate of $3F6H12A\text{-}1PFBS\bullet 118H_2O + 19$ free H_2O. Water molecules within 3.3 Å of the CF chain or 3 Å of the CH chain were considered the hydration water (Mountain and Lippa, 2008; Mountain and Thirumalai, 1998). Color for the atoms: gray balls, C; light gray balls, H; red balls, O; navy blue balls, N; cyan-blue balls, F; light yellow balls, S; light green polyhedrons, Mg; yellow polyhedrons, Si; pink polyhedrons, Al.

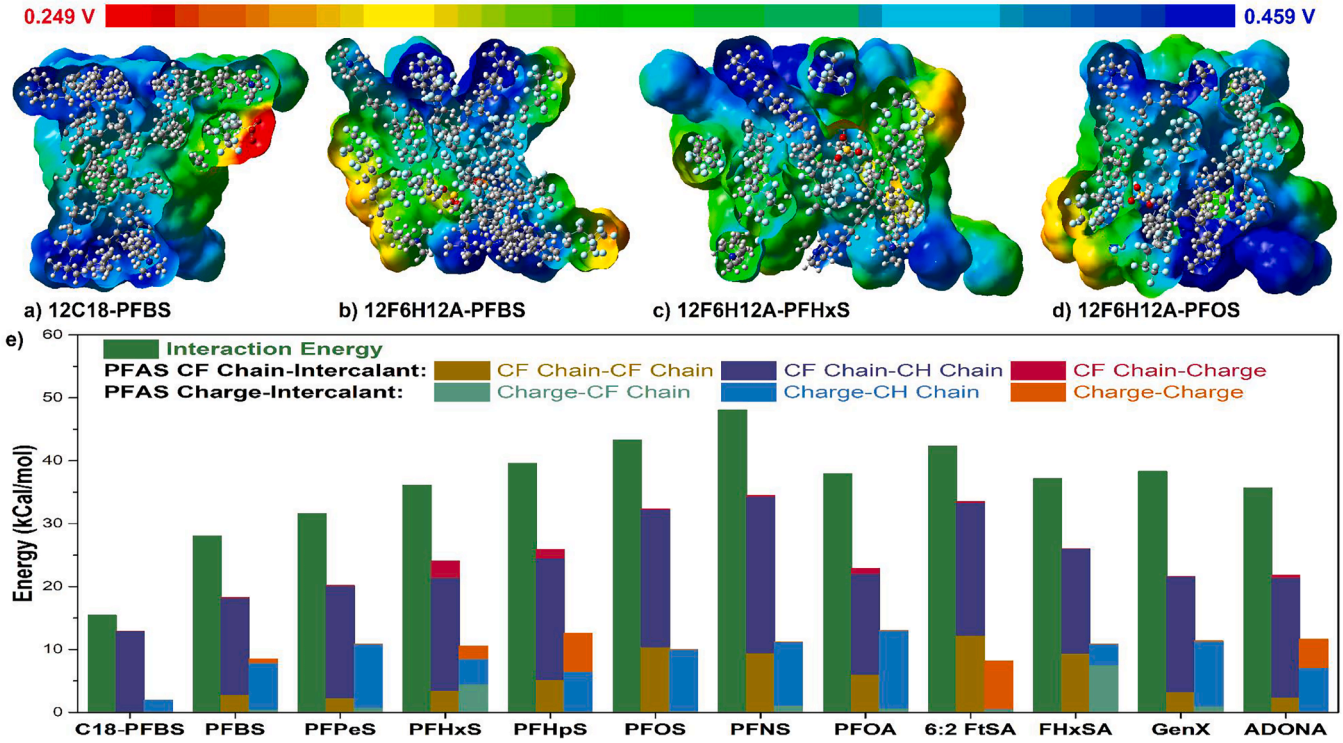

Fig. 3. Electrostatic potential map of 12C18—1PFBS (a), 12F6H12A—1PFBS (b), 12F6H12A—1PFHxS (c), 12F6H12A—1PFOS (d), configurations obtained at the 1 μs MD simulation; e) total interaction energy ΔE of 1 PFAS with 12 F6H12A and its energy decomposition.

charged quaternary ammonium group in both C18 and F6H12A was relatively low. Impressively, each interaction term of F6H12A for PFBS was more significant than that of C18 due to the high contact area with the CH-CF domain.

A second-order perturbation analysis on the natural population analysis was performed to assess the electron delocalization in the self-assembly structure. In 12F6H12A—PFBS, the lone pairs of e^- on the oxygen atoms and antibonding orbitals of S-O of PFBS interacted with the antibonding orbitals of C-H and C Rydberg orbitals in the C-H bond of F6H12A, respectively, which gave rise to the charge-CH chain energy of 7.4 kcal/mol. A strong interaction (17.3 kcal/mol) was observed between the lone pairs on F atoms in PFBS and the antibonding orbitals of the C-H bond in F6H12A. This interaction arose from the excess electron density on the fluorine atom that is partially transferred to the neighboring antibonding orbitals (Mendez-Arroyo et al., 2014). Notably, in complex 12F6H12A—6:2 FtSA, the lone pair e^- of F atom associated with the antibonding orbital of C-F bond that generated the "fluorophilic" interaction (CF chain-CF chain interaction 12.2 kcal/-mol). Stronger and more diverse interactions of F6H12A with PFAS compounds resulted in the unique "cavity" structure and boosted its adsorption performance than the traditional hydrocarbon intercalant C18.

Performance of FluoroClay for PFAS estimated by all-atom MD simulation

Finally, we sought to estimate the performance of clay modified by F6H12A (FluoroClay) for PFAS. To achieve this aim, we carried out 1 μs MD simulations of clay supercell (20 × 12 unit cells) with PFAS in SPC/E water. The ratio of cation exchange capacity to F6H12A was set to 1:1, and 48 PFAS were randomly inserted (20% of the intercalant) (Du et al., 2016). A PFAS molecule was considered to be adsorbed if it is within 3.3 Å of the intercalants (Mountain and Lippa, 2008; Mountain and Thirumalai, 1998). Consistent with reported work (Du et al., 2016), all PFAS, including PFBS, PFOS, PFOA, 6:2 FtSA, FHxSA, GenX, and ADONA assembled with F6H12A in the interlayer space, and there was no freely non-adsorbed PFAS (Fig. 4a and Fig. S16a-S21a). Fig. 4 displays the final configurations of FluoroClay-PFAS. All time series of RMSD difference are only 0.05-0.2 nm (Fig. 4b and Fig. S16b-S21b), indicating that the interlayer structure formed by F6H12A is very stable. Remarkably, the diffusion coefficients of the adsorbed PFBS, PFOS, PFOA,6:2 FtSA, FHxSA, GenX, and ADONA calculated by the mean square displacement (MSD, Fig. 4c and Fig. S16c-S21c) were $(0.0057 \pm 0.0014) \times 10^{-6}$ cm^2/s, $(0.0060 \pm 0.0007) \times 10^{-6}$ cm^2/s, $(0.0072 \pm 0.0008) \times 10^{-6}$ cm^2/s, $(0.0015 \pm 0.0005) \times 10^{-6}$ cm^2/s, $(0.0095 \pm 0.0012) \times 10^{-6}$ cm^2/s, $(0.0036 \pm 0.0013) \times 10^{-6}$ cm^2/s, $(0.0095 \pm 0.0017) \times 10^{-6}$ cm^2/s, respectively. These values were much lower (~ three orders of magnitude) than those of free PFOA (4.37×10^{-6} cm^2/s) and PFOS (5.08×10^{-6} cm^2/s) (Guan et al., 2018), implying the strong association between intercalants F6H12A and PFAS. Additionally, the mobility of F6H12A (diffusion coefficient $(0.0012 \pm 0.0001) \times 10^{-6}$ cm^2/s) was even lower than the adsorbed PFAS.

Comparison with commercial adsorbents such as activated carbon and ion exchange resin either computationally or experimentally and

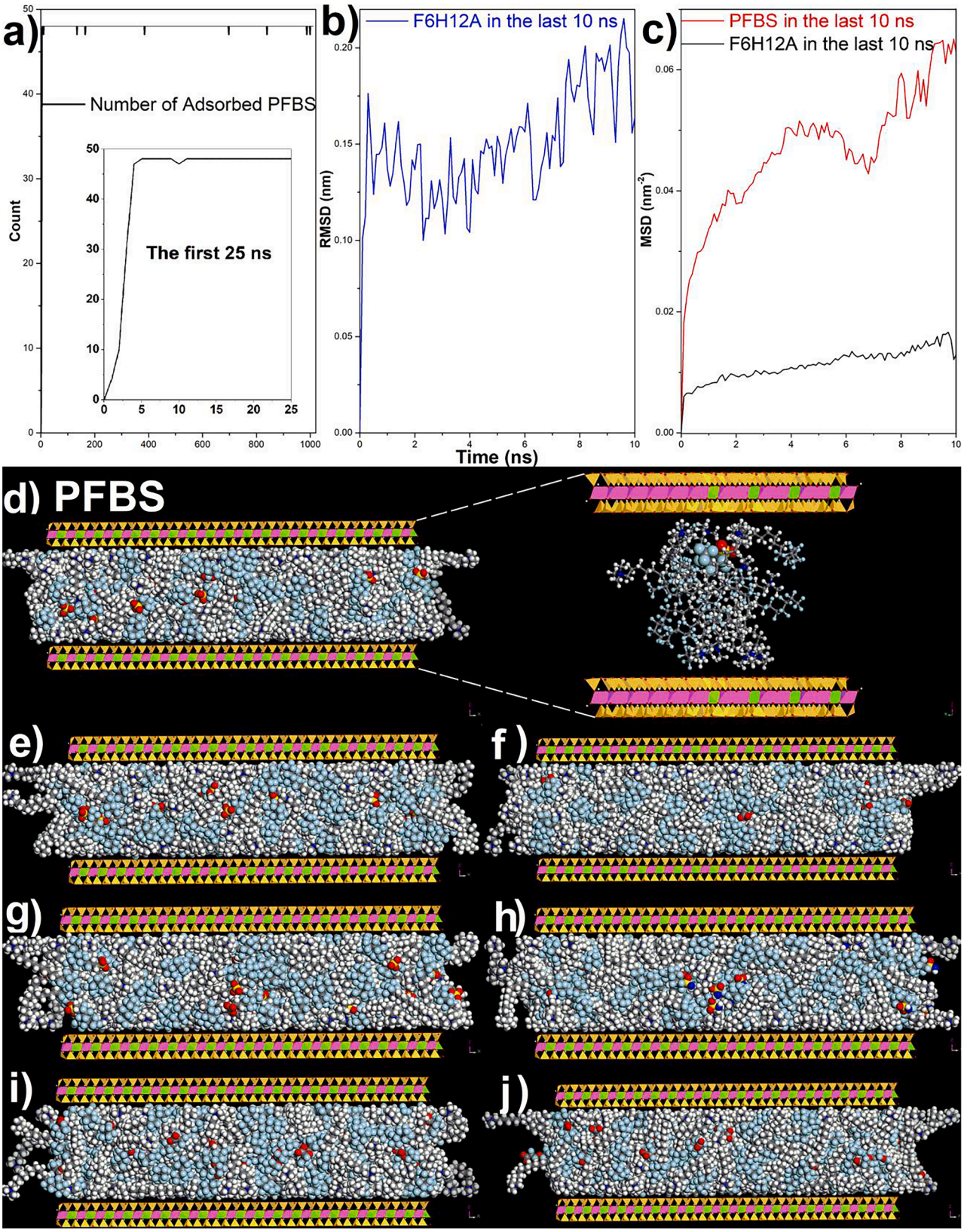

Fig. 4. a) Number of PFBS been adsorbed by FluoroClay as a function of simulation time; b) RMSD of F6H12A intercalant structure in the last 10 ns; c) MSD of adsorbate PFBS and F6H12A versus the simulation time; snapshots of FluoroClay for PFAS at 1 μs MD simulation: d) 240F6H12A—48 PFBS; e) 240F6H12A—48 PFOS; f) 240F6H12A—48 PFOA; g) 240F6H12A—48 6:2 FtSA; h) 240F6H12A—48 FHxSA; i) 240F6H12A—48 GenX; j) 240F6H12A—48 ADONA. All PFAS, including PFBS, GenX and ADONA, were assembled with F6H12A in the interlayer space, and there was no freely non-adsorbed PFAS.

the life cycle analysis of FluoroClay are meaningful and will be performed in the future. Evaluation of a variety of functionals (e.g., self-interaction corrected functionals) and simulation approaches (e.g., ab initial MD) in design of new materials would be of interest as well.

Conclusion

In conclusion, the results from MD simulation coupled with DFT-based computation demonstrated the possibility of rationally selecting intercalants to design a clay-based material and estimate its performance. F6H12A-modified clay revealed robust adsorption affinity for PFAS, especially PFBS, GenX, and ADONA. The adsorption behavior of PFAS in the interlayer of (modified) smectite clay could be concluded as the self-assembly of intercalant-PFAS under the negative electric field of clay sheets, which is thermodynamically entropy-driven and dominated by hydrophobic effect. Introducing fluorine atoms gave rise to a hydrophobic and fluorophilic "cavity" structure for PFAS. The unique configuration originated from their intensified intermolecular interactions and enlarged the release of low entropy hydration water into the bulk solution. Based on the DFT-based energy decomposition, we demonstrated that the interactions involving CF chains (CF chain-CH chain and CF chain-CF chain) contributed to a large proportion of the total ΔE, while the ionic interaction between the positively charged quaternary ammonium group in both C18 and F6H12A with PFAS was relatively low ($< 5\%$ in most cases). The methodologies demonstrated in this study can also be used to design other sorbent materials, especially for removing highly fluorinated contaminants with unique chemistry prior to attempting laboratory synthesis.

Appendix A. Supplementary data

The details of MD simulation and DFT-based calculations and comparison of FnH12A can be found in the Supporting information.

Declaration of Competing Interest

The authors declare no competing financial interest.

Data availability

Data will be made available on request.

Acknowledgments

This project is funded by the NSERC Collaborative Research & Development Grant (CRDPJ 537771-18) and Discovery Accelerator Supplements Program (RGPAS-2018-522617). The molecular dynamics simulation and Gaussian calculation were performed on the Cedar cluster of Compute Canada.

Supplementary materials

Supplementary material associated with this article can be found, in the online version, at doi:10.1016/j.wroa.2023.100175.

References

Adcock, S.A., McCammon, J.A., 2006. Molecular dynamics: Survey of methods for simulating the activity of proteins. Chem. Rev. 106 (5), 1589–1615.
Ateia, M., Alsbaiee, A., Karanfil, T., Dichtel, W., 2019. Efficient PFAS removal by amine-functionalized sorbents: critical review of the current literature. Environ. Sci. Technol. Lett. 6 (12), 688–695.
Backe, W.J., Field, J.A., Day, T.C., 2013. Zwitterionic, cationic, and anionic fluorinated chemicals in aqueous film forming foam (AFFF) formulations and groundwater from U.S. military bases by non-aqueous large-volume injection HPLC-MS/MS. Environ. Sci. Technol. 47 (10), 5226–5234.
Berendsen, H.J.C., Grigera, J.R., Straatsma, T.P., 1987. The missing term in effective pair potentials. J. Phys. Chem. 91 (24), 6269–6271.
Biswas, S., Yamijala, S.S.R.K.C., Wong, B.M., 2022. Degradation of per- and polyfluoroalkyl substances with hydrated electrons: A new mechanism from first-principles calculations. Environ. Sci. Technol. 56 (12), 8167–8175.
Boyer, T.H., Fang, Y., Ellis, A., Dietz, R., Choi, Y.J., Schaefer, C.E., Higgins, C.P., Strathmann, T.J., 2021. Anion exchange resin removal of per- and polyfluoroalkyl substances (PFAS) from impacted water: A critical review. Water Res. 200, 117244.
Buck, R.C., Franklin, J., Berger, U., Conder, J.M., Cousins, I.T., de Voogt, P., Jensen, A.A., Kannan, K., Mabury, S.A., van Leeuwen, S.P., 2011. Perfluoroalkyl and polyfluoroalkyl substances in the environment: terminology, classification, and origins. Integr. Environ. Assess. Manage. 7 (4), 513–541.
Cadars, S., Guégan, R., Garaga, M.N., Bourrat, X., Le Forestier, L., Fayon, F., Huynh, T.V., Allier, T., Nour, Z., Massiot, D., 2012. New insights into the molecular structures, compositions, and cation distributions in synthetic and natural montmorillonite clays. Chem. Mater. 24 (22), 4376–4389.
Du, Z., Deng, S., Zhang, S., Wang, B., Huang, J., Wang, Y., Yu, G., Xing, B., 2016. Selective and high sorption of perfluorooctanesulfonate and perfluorooctanoate by fluorinated alkyl chain modified montmorillonite. J. Phys. Chem. C 120 (30), 16782–16790.
Grimme, S., Antony, J., Ehrlich, S., Krieg, H., 2010. A consistent and accurate ab initio parametrization of density functional dispersion correction (DFT-D) for the 94 elements H-Pu. J. Phys. Chem. 132 (15), 154104.
Guan, D.-X., Li, Y.-Q., Yu, N.-Y., Yu, G.-H., Wei, S., Zhang, H., Davison, W., Cui, X.-Y., Ma, L.Q., Luo, J., 2018. In situ measurement of perfluoroalkyl substances in aquatic systems using diffusive gradients in thin-films technique. Water Res. 144, 162–171.
Hermann, J., DiStasio, R.A., Tkatchenko, A., 2017. First-Principles models for van der Waals interactions in molecules and materials: concepts, theory, and applications. Chem. Rev. 117 (6), 4714–4758.
Hidalgo, A., Mora-Diez, N., 2016. Novel approach for predicting partition coefficients of linear perfluorinated compounds. Theor. Chem. Acc. 135 (1), 18.
Houtz, E.F., Higgins, C.P., Field, J.A., Sedlak, D.L., 2013. Persistence of perfluoroalkyl acid precursors in AFFF-Impacted groundwater and soil. Environ. Sci. Technol. 47 (15), 8187–8195.
Jing, P., Rodgers, P.J., Amemiya, S., 2009. High lipophilicity of perfluoroalkyl carboxylate and sulfonate: Implications for their membrane permeability. J. Am. Chem. Soc. 131 (6), 2290–2296.
Kissa, E., 2001. Fluorinated Surfactants and Repellents. Marcel Dekker, Inc, New York, NY.
Krafft, M.P., Riess, J.G., 2009. Chemistry, physical chemistry, and uses of molecular fluorocarbon–hydrocarbon diblocks, triblocks, and related compounds—unique "apolar" components for self-assembled colloid and interface engineering. Chem. Rev. 109 (5), 1714–1792.
Krafft, M.P., Riess, J.G., 2015. Selected physicochemical aspects of poly- and perfluoroalkylated substances relevant to performance, environment and sustainability—Part one. Chemosphere 129, 4–19.
Kumarasamy, E., Manning, I.M., Collins, L.B., Coronell, O., Leibfarth, F.A., 2020. Ionic fluorogels for remediation of per- and polyfluorinated alkyl substances from water. ACS Cent. Sci. 6 (4), 487–492.
Liu, J., Van Hoomissen, D.J., Liu, T., Maizel, A., Huo, X., Fernández, S.R., Ren, C., Xiao, X., Fang, Y., Schaefer, C.E., Higgins, C.P., Vyas, S., Strathmann, T.J., 2018. Reductive defluorination of branched per- and polyfluoroalkyl substances with cobalt complex catalysts. Environ. Sci. Technol. Lett. 5 (5), 289–294.
Maestre, A., Guardado, P., Moyá, M.L., 2014. Thermodynamic study of bile salts micellization. J. Chem. Eng. Data 59 (2), 433–438.
Mendez-Arroyo, J., Barroso-Flores, J., Lifschitz, A.M., Sarjeant, A.A., Stern, C.L., Mirkin, C.A., 2014. A multi-state, allosterically-regulated molecular receptor with switchable selectivity. J. Am. Chem. Soc. 136 (29), 10340–10348.
Moody, C.A., Hebert, G.N., Strauss, S.H., Field, J.A., 2003. Occurrence and persistence of perfluorooctanesulfonate and other perfluorinated surfactants in groundwater at a fire-training area at Wurtsmith Air Force Base, Michigan, USA. J. Environ. Monitor. 5 (2), 341–345.
Mountain, R.D., Lippa, K.A., 2008. Solvation of perfluorooctane and octane in water, methanol, acetonitrile, and aqueous mixtures of methanol and acetonitrile. J. Phys. Chem. B 112 (26), 7785–7793.
Mountain, R.D., Thirumalai, D., 1998. Hydration for a series of hydrocarbons. Proc. Natl. Acad. Sci. USA 95 (15), 8436–8440.
Munoz, G., Liu, M., Vo Duy, S., Liu, J., Sauvé, S., 2023. Target and nontarget screening of PFAS in drinking water for a large-scale survey of urban and rural communities in Québec, Canada. Water Res 223, 119750.
Munoz, G., Ray, P., Mejia-Avendaño, S., Vo Duy, S., Tien Do, D., Liu, J., Sauvé, S., 2018. Optimization of extraction methods for comprehensive profiling of perfluoroalkyl and polyfluoroalkyl substances in firefighting foam impacted soils. Anal. Chim. Acta 1034, 74–84.
Park, M., Wu, S., Lopez, I.J., Chang, J.Y., Karanfil, T., Snyder, S.A., 2020. Adsorption of perfluoroalkyl substances (PFAS) in groundwater by granular activated carbons: Roles of hydrophobicity of PFAS and carbon characteristics. Water Res. 170, 115364.
Phillips, J.N., 1955. The energetics of micelle formation. Trans. Faraday Soc. 51 (0), 561–569.
Ruiz-Hitzky, E., Van Meerbeek, A., 2006. Clay Mineral– and Organoclay–Polymer Nanocomposite. In: Bergaya, F., Theng, B.K.G., Lagaly, G. (Eds.), Developments in Clay Science. Elsevier, pp. 583–621.
U.S. EPA, 2021. PFAS Strategic Roadmap: EPA's Commitments to Action 2021-2024.
U.S. EPA, 2022. Drinking Water Health Advisories for PFAS Fact Sheet for Communities.

U.S. NIST, 2022. Average bond length differences by model chemistry. Computational Chemistry Comparison and Benchmark DataBase. https://cccbdb.nist.gov/bondlengthmodel1.asp. accessed January 2nd 2023.

Xiao, L., Ling, Y., Alsbaiee, A., Li, C., Helbling, D.E., Dichtel, W.R., 2017. β-Cyclodextrin polymer network sequesters perfluorooctanoic acid at environmentally relevant concentrations. J. Am. Chem. Soc. 139 (23), 7689–7692.

Yamijala, S.S.R.K.C., Shinde, R., Wong, B.M., 2020. Real-time degradation dynamics of hydrated per- and polyfluoroalkyl substances (PFASs) in the presence of excess electrons. Phys. Chem. Chem. Phys. 22 (13), 6804–6808.

Yan, B., Munoz, G., Sauve, S., Liu, J., 2020. Molecular mechanisms of per- and polyfluoroalkyl substances on a modified clay: A combined experimental and molecular simulation study. Water Res. 184, 116166.

Yan, B., Wang, J., Liu, J., 2021. STXM-XANES and computational investigations of adsorption of per- and polyfluoroalkyl substances on modified clay. Water Res. 201, 117371.

Yang, A., Ching, C., Easler, M., Helbling, D.E., Dichtel, W.R., 2020. Cyclodextrin polymers with nitrogen-containing tripodal crosslinkers for efficient PFAS adsorption. ACS Mater. Lett. 2 (9), 1240–1245.

Zeng, Q.H., Yu, A.B., Lu, G.Q., Standish, R.K., 2003. Molecular dynamics simulation of organic−inorganic nanocomposites: Layering behavior and interlayer structure of organoclays. Chem. Mater. 15 (25), 4732–4738.